Crystal structure analysis from powder X-ray diffraction data using high-temperature attachment for capillaries

Hisashi Konaka* and Akito Sasaki*

1. Introduction

The physical and chemical properties of a crystalline solid depend heavily on the conformations of the molecules and the arrangement of atoms and molecules, that is, the "crystal structure", as well as on the composing elements and molecular structures. The single crystal structure analysis technique is used in many fields as a good tool to precisely clarify the crystal structures required to understand the mechanisms of developing physical properties of crystalline materials.

In recent years, reports of the success of crystal structure analysis from powder X-ray diffraction data are increasing, particularly in regards to polycrystalline samples that were difficult for single crystal structure analysis. In addition to improvements in analysis methods and high performance PCs, one of the major reasons is that very good diffraction data can now be obtained using in-house powder X-ray diffractometers instead of synchrotron facilities due to improvements in X-ray optical devices and detectors.

In particular, there has been increased interest in materials whose physical properties change due to an external field because these materials have applications relating to switching devices, sensors, memory materials, and so forth. For these external field active materials, solving the crystal structures is crucial to elucidating the mechanisms of physical property changes. So far, numerous single crystal analysis results have been reported for external field active crystals *before* response to the external field. However, most of the crystal structures *after* response to the external field have not been solved because the single crystal state usually collapses during phase transitions brought about by the changes in physical properties.

It is worth solving the crystal structures of these materials *after* response to the external filed using powder X-ray diffraction data to elucidate physical properties and to obtain new knowledge about physical properties. This requires a method of measurement while the external field is maintained.

The "High-temperature attachment for capillaries" is an attachment to be used in powder X-ray diffraction measurement. This attachment has the following two features:

(1) The sample can be heated. Powder X-ray diffraction data can be collected at a specified temperature. Diffraction data from the sample after phase transition or crystalline phases change by heating can also be collected.

(2) The polycrystalline sample in a glass capillary can be measured while it spins. If you fill the indent of a glass sample holder with polycrystalline sample, the intensity ratios between one diffraction and another often change due to preferred orientations, which makes crystal structure analysis difficult. The degree of preferred orientations is reduced by spinning the capillary samples; therefore, you will be able to obtain data of high enough quality for crystal structure analysis.

The Ni(II) complex with the *N*,*N*-diethylethylenediamine (Et_2en) ligand (Fig. 1) shows structural changes during heating. It has been known since 1963[1] that this complex exhibits color changes based on hydration/dehydration transitions and thermochromism depending on the selected anion[2]–[7]. Many researchers performed detailed analyses of this complex. However, crystal structures of most of the complexes have not been solved after the structural changes. The only crystal structures that have been solved are in cases where the single crystals survived the phase change[7].

In this article, from among the various Ni(II)-Et_2en complexes, $[Ni(Et_2en)_2(H_2O)_2]Cl_2$, $[Ni(Et_2en)_2]Br_2$ and $[Ni(Et_2en)_2](BF_4)_2$ were selected, and hereafter are described the results of the crystal structure analyses using the high-temperature attachment for capillaries for the purpose of elucidating the transition behaviors based on the powder X-ray crystal structure analysis.

2. Measurement and analysis

All the powder X-ray diffraction measurements were performed using the SmartLab automated multipurpose X-ray diffractometer.

In order to get rough information on structural changes with temperature and to decide on the measurement temperature for powder X-ray crystal structure analysis, powder X-ray diffraction measurement was performed

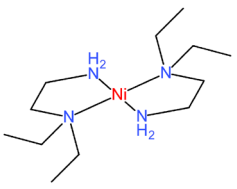

Fig. 1. Molecular structure of $[Ni(Et_2en)_2]^{2+}$.

* XRD Application & Software Development, X-ray Analysis Division, Rigaku Corporation.

using the X-ray DSC attachment (Fig. 2). With this attachment, both DSC and X-ray diffraction data can be collected simultaneously while temperature and humidity are adjusted.

The measurements for crystal structure analysis were performed using focusing beam optics[8], where the Cu$K\alpha_1$ X-rays, monochromatized by the Kα1 unit, are line-focused on the detector window using the CBO-E unit. A glass capillary was filled with sample, which was then measured at a specified temperature using the high-temperature attachment for capillaries (Fig. 3).

PDXL Integrated Powder X-ray Diffraction Software[9],[10] was used for the crystal structure analysis from powder diffraction data.

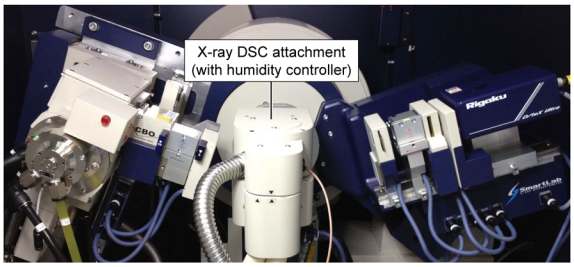

Fig. 2. X-ray diffractometer equipped with an X-ray DSC attachment.

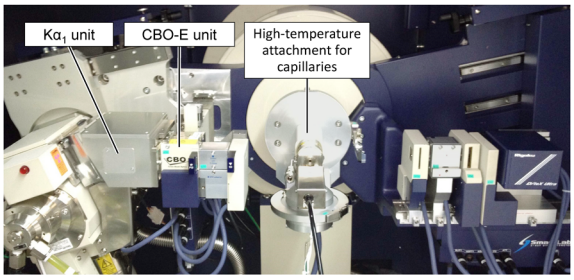

Fig. 3. X-ray diffractometer equipped with a high-temperature attachment for capillaries.

3. Hydration/dehydration transition of $[Ni(Et_2en)_2(H_2O)_2]Cl_2$

As shown in Fig. 4, $[Ni(Et_2en)_2(H_2O)_2]Cl_2$ (**1a**), light-blue crystals, shows a dehydration transition during heating[2]; **1a** turns to $[Ni(Et_2en)_2(H_2O)_2]Cl_2$ (**1b**) in which chloride ions coordinate with the Ni(II) ions. While the crystal structure of **1a** has been reported[11], the structure after dehydration transition has not been reported yet.

Figure 5 shows the simultaneous XRD & DSC measurement results of **1a** under heating and humidification. **1a** showed an endothermic reaction at 361 K after heating from room temperature, and eventually gave the X-ray diffraction patterns of a crystalline phase considered to be **1b**. Since no other crystalline or amorphous phases were observed around the time of the reaction, it turned out that **1a** underwent the crystal-to-crystal dehydration transition to generate **1b**. After cooling the generated **1b** down to 300 K, the surrounding humidity was changed from 5%RH to 70%RH at 300 K. As a result, the diffraction pattern of **1b** changed at 25%RH with exotherm. The diffraction peaks of **1b** eventually disappeared and the diffraction pattern returned to that of **1a**. Thus, it was clarified that **1b** turned into **1a** by exposing **1b** to water vapor. Here, **1a**′ is the crystalline phase generated by way of **1b**. In

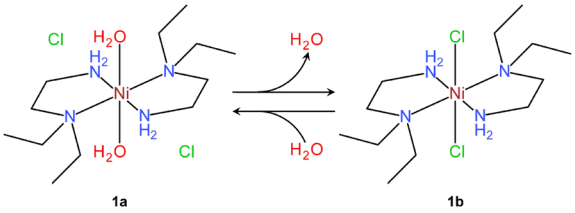

Fig. 4. Structural changes between **1a** and **1b**.

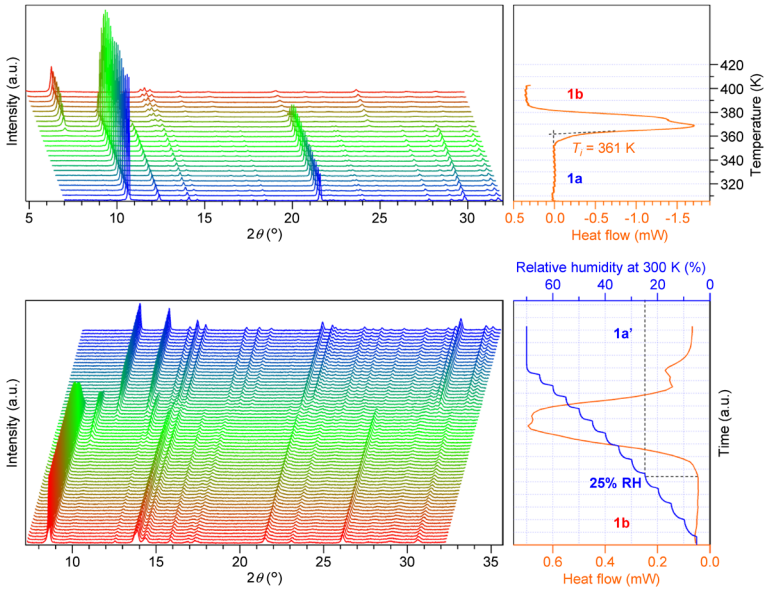

Fig. 5. The results of XRD & DSC measurement; during heating **1a** (upper), during humidifying **1b** (bottom).

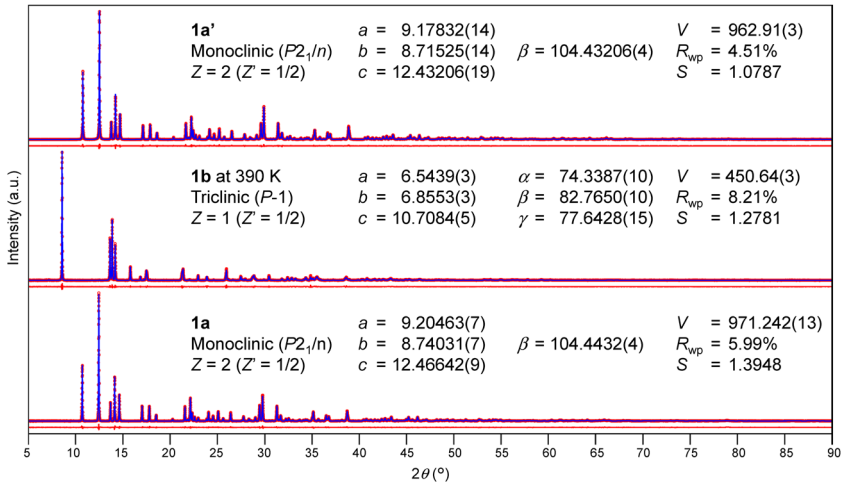

Fig. 6. Collected XRD profiles, calculated profiles, and determined unit cell parameters of **1a**, **1b** and **1a′**.

the middle of the transition from **1b** to **1a′**, two peaks were observed at $2\theta = 10°$ and 13°, neither of which could be assigned to the crystalline phases, and the crystal structure could not be analyzed.

Next, the crystal structure analyses of **1a**, **1b**, and **1a′** were performed from their powder diffraction data collected using the high-temperature attachment for capillaries. For **1b**, the measurement was done at 390 K, after the endothermic reaction caused by dehydration was completed. Figure 6 shows the measurement data, calculated data and difference plot of each compound. In each result, the calculated data was in good agreement with the measurement data. While the crystal structure of **1a**, which is already known, is monoclinic, $P2_1/n$, that of **1b** is triclinic, P-1. The crystal structure of **1a′** was confirmed to have the same unit cell parameters and the same space group as **1a**.

Figure 7 shows the results of crystal structure analysis from powder X-ray diffraction data. The water molecules in **1a** are coordinated in the axial direction of the $[Ni(Et_2en)_2]^{2+}$. Adjacent complex molecules were connected by hydrogen bonds via free chlorides and formed two-dimensional sheet structures. Here, the amino groups of the Et_2en ligands were not involved in hydrogen bond formation. Chlorides were coordinated to the Ni atoms in the crystal structure of **1b,** which was obtained by heating and dehydration. The complex molecules formed two-dimensional sheet structures through hydrogen bonds between amino groups and chlorides of adjacent complex molecules. As shown at the bottom-right of Fig. 7, a disordered structure was found in the conformation of the Et_2en molecules in **1b**. The site occupancies of the two types of conformation were 64.9% and 35.1%, respectively. **1a′**, obtained by hydration of **1b**, was confirmed to have the same crystal structure as **1a**.

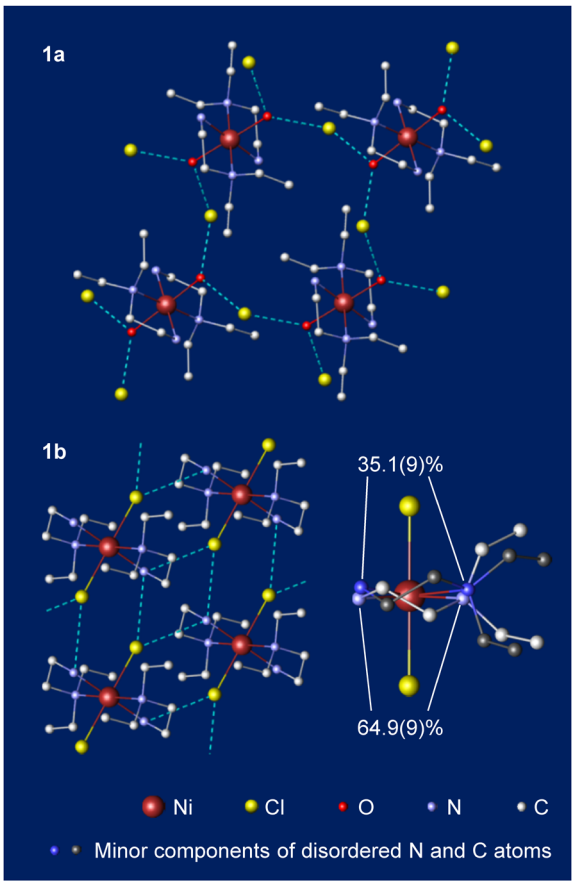

Fig. 7. Crystal structure of **1a** (upper) and **1b** (bottom-left), and disordered structure of Et_2en molecule in **1b** (bottom-right). In the crystal structure of **1b**, the disordered Et_2en molecules are omitted.

4. Hydration/dehydration and structural phase transition of $[Ni(Et_2en)_2]Br_2$

As shown in Fig. 8, it is known that $[Ni(Et_2en)_2]Br_2$ (**2a**) undergoes a hydration transition to result in $[Ni(Et_2en)_2]Br_2$ (**2b**), where water molecules coordinate to Ni(II) by humidification[2]. Although the crystal structure of **2a** has already been reported[12], the crystal structure after the hydration transition has not been reported yet.

Figure 9 shows the results of XRD and DSC measurements of **2a** during heating and humidifying.

The diffraction pattern of **2a** converted to that of a different complex considered to be **2b** at 30%RH with exotherm as a result of humidifying the sample from 5%RH to 70%RH at 300 K. Subsequent heating of **2b** from room temperature caused an endothermic reaction at 344 K to provide a new crystalline phase **2c** with a different diffraction pattern from that of **2a**. Further heating returned the diffraction pattern of the new phase **2c** to that of **2a**, without a big change in the DSC chart in the temperature range from 390 K to 400 K, although there was a big change in the diffraction pattern. This clarified that **2c** underwent a structural phase transition during heating. Because no crystalline or amorphous phases other than **2a**, **2b**, **2c**, and **2a′** were observed around the time of each reaction, **2a**, **2b**, and **2c** turned out to undergo the crystal-to-crystal hydration/dehydration/structural phase transitions, respectively.

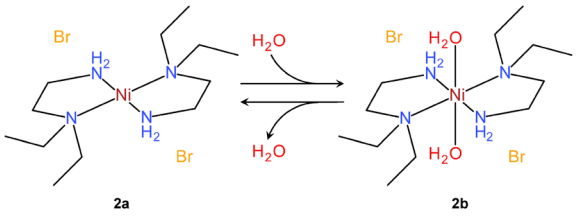

Fig. 8. Structural changes between **2a** and **2b**.

Next, the crystal structure analysis of **2a**, **2b**, **2c**, and **2a′** were determined from powder X-ray diffraction data as described in the previous section (Fig. 10). The diffraction measurements were made for **2a** and **2b** at room temperature, **2c** at 350 K, and **2a′** at 400 K. By the way, when **2c** was prepared by heating and dehydrating **2b**, about 26% of **2c** turned to **2a′** by a structural phase transition. However, we succeeded in the structure analysis of **2c** by taking into account the fact that the diffraction pattern was obtained from a mixture of **2a′**

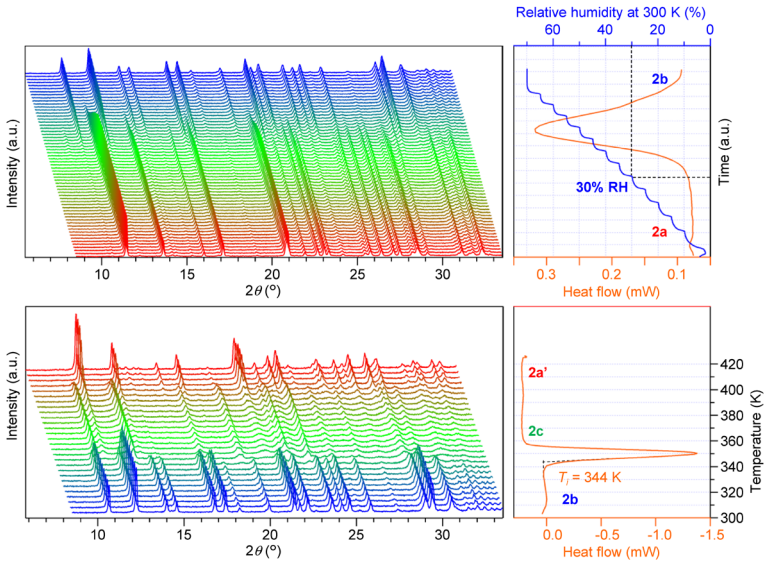

Fig. 9. The results of XRD & DSC measurement; during humidifying **2a** (upper), during heating **2b** (bottom).

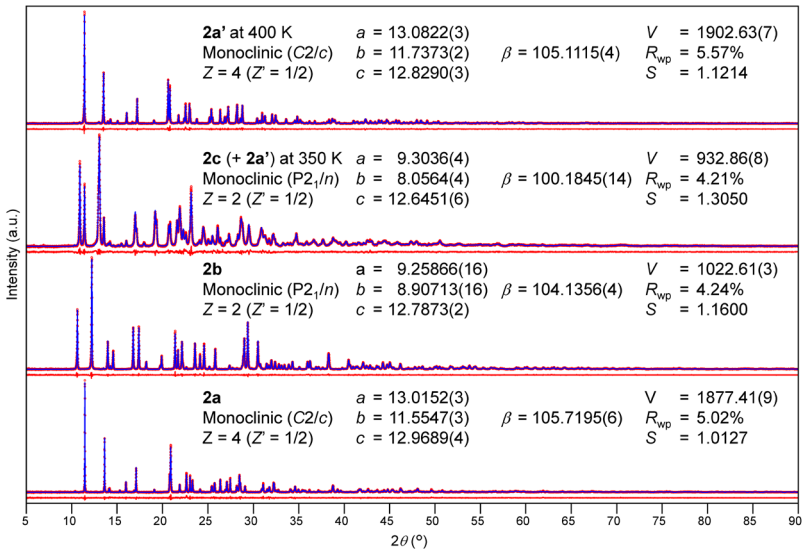

Fig. 10. Collected XRD profiles, calculated profiles, and determined unit cell parameters of **2a**, **2b**, **2c** and **2a′**.

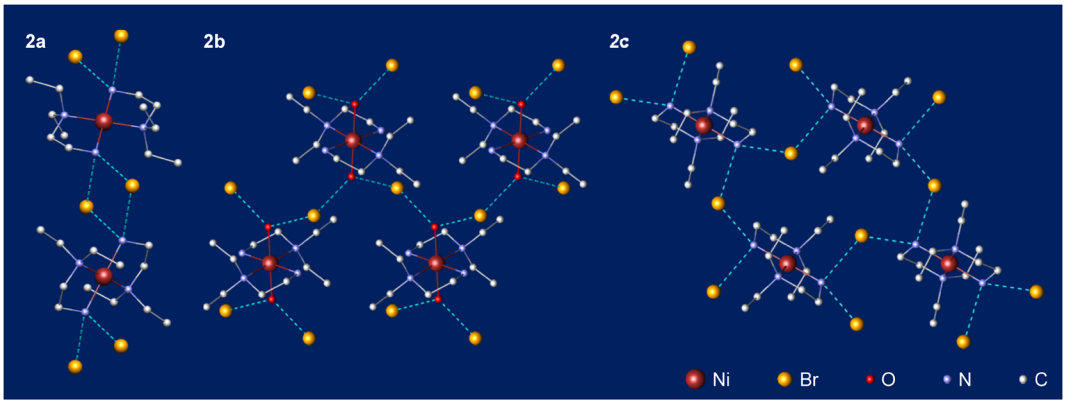

Fig. 11. Crystal structure of **2a** (left), **2b** (middle), and **2c** (right).

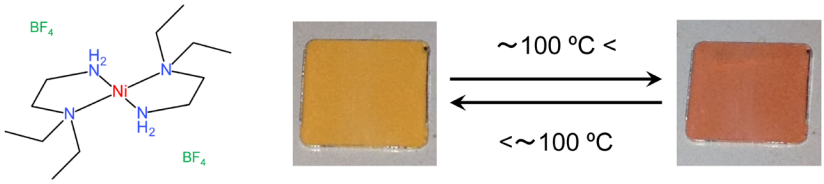

Fig. 12. Molecular structure of **3a** and a demonstration of its thermochromism.

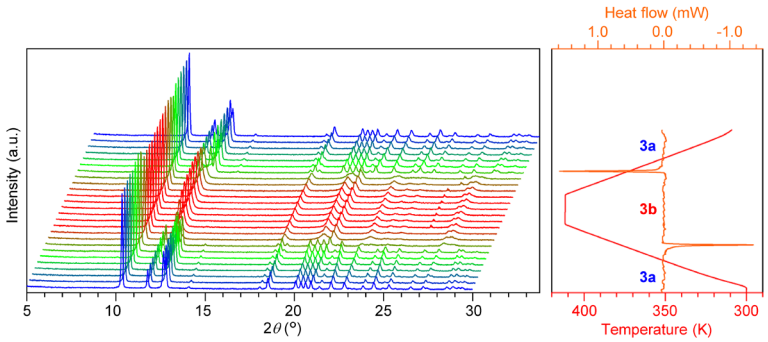

Fig. 13. Results of XRD & DSC measurements of **3a** during heating and cooling.

and **2c**. While the crystal structure of **2a** is monoclinic, $C2/c$, the space group of **2b** was $P2_1/n$. The phase **2c** obtained by heating and dehydrating **2b** caused a structural phase transition without changing space groups. Furthermore, although the unit cell became a little larger because the measurement was made at high temperature, the diffraction pattern of **2a′** obtained by heating **2c** was very similar to that of **2a** and the space group returned to that of **2a**.

The results obtained by powder X-ray crystal structure analysis are shown in Fig. 11. The Ni^{2+} ions of **2a** form a square planar structure that has two Et_2en molecules coordinated but no bromides coordinated. Adjacent complex molecules were connected through hydrogen bonds via free bromides and formed one-dimensional chains. **2a**, generated after hydration transition by humidification, formed an octahedral structure where water molecules coordinated to the square planar Ni-Et_2en complex from the axial direction. **2b** had a similar packing structure to that of **1a**, where the amino groups of the Et_2en ligands were not involved in the hydrogen bonds but the water molecules and bromide ions formed hydrogen bonds. **2c**, obtained by dehydration transition of **2b**, had a similar molecular structure to that of **2a**, but caused a very different hydrogen bond formation to produce a two-dimensional sheet structure. The crystal structure of **2a′** was the same as that of **2a**.

5. Structural phase transition of $[Ni(Et_2en)_2](BF_4)_2$

$[Ni(Et_2en)_2](BF_4)_2$ (**3a**), orange crystals at room temperature, shows thermochromism in that the orange crystals suddenly turn to red crystals upon heating as shown in Fig. 12[(1),(3)]. Details of the thermochromism of **3a** have been clarified by many researchers, but the crystal structures of the low-temperature phase **3a** and the high-temperature phase **3b** have not been solved because it was not possible to prepare any single crystals large enough to measure.

Figure 13 shows the results of the simultaneous XRD and DSC measurements of **3a** under heating and cooling conditions. As reported by S. Hayami *et al.*[(7)],

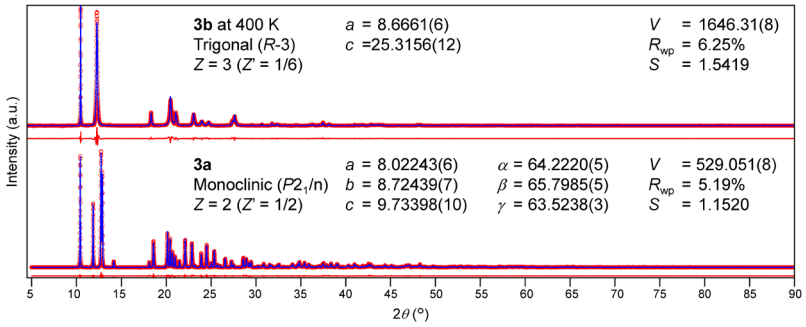

Fig. 14. Collected XRD profiles, calculated profiles, and determined unit cell parameters of **3a** and **3b**.

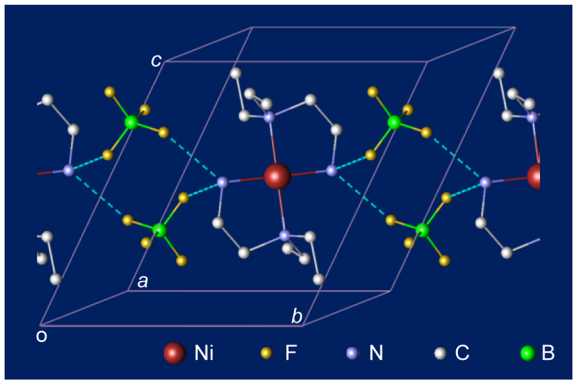

Fig. 15. Crystal structure of **3a**.

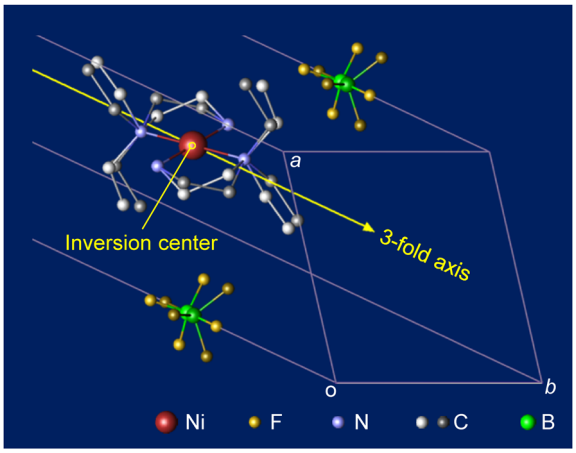

Fig. 16. Crystal structure of **3b**. The atoms in the asymmetric unit and those generated by symmety are displayed.

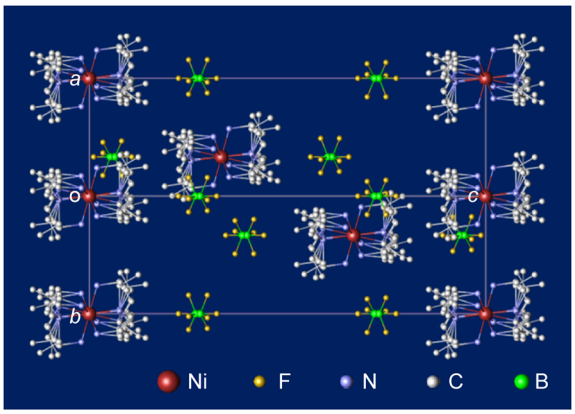

Fig. 17. Crystal structure of **3b**.

we confirmed that the endothermic and exothermic reactions occurred at 376 K and 374 K when heating and cooling, respectively. Since no crystalline or amorphous phases other than **3a** and **3b** were observed, this reaction turned out to be the crystal-to-crystal structural phase transition.

As in the previous report, the crystal structures of **3a** and **3b** were analyzed based on their powder diffraction data (Fig. 14). The diffraction pattern of **3a** was very similar to that of $[Cu(Et_2en)_2](BF_4)_2$[13]. The powder diffraction pattern of **3b** was obtained from the measurement at 400 K. The analysis result elucidated that the unit cell volume was 1646 Å^3, and that the crystal system was trigonal or hexagonal.

Figure 15 shows the result obtained from the powder X-ray crystal structure analysis of **3a**. The space group of **3a** was triclinic, *P*-1, and the Ni atoms were located on the symmetric centers. The complex molecules were connected by two molecules of tetrafluoroborate through hydrogen bonds and formed a one-dimensional chain structure. This crystal structure was isomorphic with that of $[Ni(Et_2en)_2](ClO_4)_2$[6], $[Cu(Et_2en)_2](ClO_4)_2$[14],[15], and $[Cu(Et_2en)_2](BF_4)_2$.

In the crystal structure analysis of **3b**, structure determination was attempted with several possible space groups based on the systematic absences in the diffraction patterns. As a result, the measurement data was in good agreement with the data calculated when trigonal, *R*-3 was selected. The asymmetric unit volume is one-eighteenth of the unit cell volume in the space group *R*-3. The unit cell volume was almost equivalent to that of three complex molecules; in other words, one-sixth of the complex molecule existed in the asymmetric unit.

It was reported that the chelate ring composed of Ni and Et_2en of **3b** caused δ–λ puckering, based on the measurement results of solid state ^{2}H NMR[6]. Therefore, the crystal structure of **3b** was determined and refined by assuming that a disordered structure between the δ and λ forms could exist. The result showed that the Ni atoms were located on the symmetric centers and three-fold axes, and that the complex molecules were packed in

three directions randomly (Fig. 16). The tetrafluoroborate molecules were located on the same three-fold axes as $[Ni(Et_2en)_2]^{2+}$ such that $[Ni(Et_2en)_2]^{2+}$ was positioned between the tetrafluoroborate molecules. There were hydrogen bonds between the amino groups in the Et_2en ligand and tetrafluoroborate molecules, and they formed two-dimensional sheet structures parallel to the *ab* plane (Fig. 17).

6. Conclusion

We could demonstrate that the crystal structure analysis technique from powder diffraction data is very useful and effective when the single crystal state cannot be maintained due to structural phase transitions, *etc.* as well as when a certain size and quality of crystals cannot be prepared. We also collected high-quality data for crystal structure analysis at temperatures above room temperature using the high-temperature attachment for capillaries. This attachment is very useful for structure analysis after the changes in crystalline phases by heating.

By using the X-ray DSC attachment, understanding the outline of the structural changes played an important role in the crystal structure analysis.

The crystalline phase transition from **2b** to **2c**, in particular, was not elucidated in previous papers and articles because heating and dehydrating **2b** leads ultimately to sample **2a′** without much evidence of another phase in the DSC measurements. Therefore, the existence of **2c** went undetected, so its structure was not determined until now.

As described above, powder X-ray crystal structure analysis is a very powerful tool; however, you have to bear in mind that this technique is not versatile/perfect as is the case in other analysis methods. For instance, there was a trial and error approach in determining the initial structures with several space groups. The results of the solid state ^2H NMR had to be used for the structure refinement. Thus, trial and error methods and results obtained from other analysis tools sometimes have to be combined with the structure analysis from powder diffraction data.

Last but not least, crystal structure analysis results are always inevitable in elucidating physical properties from the structure point of view. We hope to gain a much better understanding of the relations between crystal structures and physical properties by solving unknown crystal structures under various measurement conditions in future.

References

(1) D. M. L. Goodgame, L. M. Venanzi: *J. Chem. Soc.*, (1963), 616−627.
(2) R. Tsuchiya, S. Joba, A. Uehara, E. Kyuno: *Bull. Chem. Soc. Jpn.*, **46** (1973), 1454−1456.
(3) L. Fabbrizzi, M. Micheloni, P. Paoletti: *Inorg. Chem.*, **13** (1974), 3019−3021.
(4) J. R. Ferraro, L. J. Basile, L. R. G-Ineguez, P. Paoletti, L. Fabbrizzi: *Inorg. Chem.*, **15** (1976), 2342−2345.
(5) S. Mitra, G. De, N. R. Chaudhuri: *Thermochimica Acta*, **66** (1983), 187−195.
(6) R. Ikeda, K. Kotani, H. Ohki, S. Ishimaru, K. Okamoto, A. Ghosh: *J. Mol. Struct.*, **345** (1995), 159−165.
(7) S. Hayami, D. Urakami, S. Sato, Y. Kojima, K. Inoue, M. Ohba: *Chem. Lett.*, **38** (2009), 490−491.
(8) A. Nedu: *Rigaku Journal (English version)*, **28** (2012), No. 2, 5−10.
(9) *Rigaku Journal (English version)*, **26** (2010), No. 1, 23−27.
(10) A. Sasaki, A. Himeda, H. Konaka, N. Muroyama: *Rigaku Journal (English version)*, **26** (2010), No. 2, 10−14.
(11) Y. Ihara, Y. Satake, Y. Fujimoto, H. Senda, M. Suzuki and A. Uehara: *Bull. Chem. Soc. Jpn.*, **64** (1991), 2349−2352.
(12) S. J. Ferrara, J. T. Mague and J. P. Donahue: *Acta Cryst.*, **E67** (2011), m48−m49.
(13) B. Narayanan, M. M. Bhadbhade: *J.Coord.Chem.*, **46**, (1998), 115−123.
(14) I. Grenthe, P. Paoletti, M. Sandström and S. Glikberg: *Inorg. Chem.*, **18**, (1979), 2687−2692.
(15) P. Naumov, K. Sakurai, T. Asaka, A. A. Belik, S. Adachi, J. Takahashi and S. Koshihara: *Inorg. Chem.*, **45**, (2006), 5027−5033.